文章编号：1001-9014(2023)01-0050-11

DOI:10. 11972/j. issn. 1001-9014. 2023. 01. 008

Efficient information acquisition spectral imaging system based on multi-field slits

LIU Shi-Jie[1,2], ZHANG Xing-Yu[1], ZHOU Hao[1], LI Chun-Lai[1,2], LI Dong Jing[1], QI Hong-Xing[1,2*], WANG Jian-Yu[1,2,3*]

(1. Hangzhou Institute for Advanced Study, University of Chinese Academy of Sciences, Hangzhou 310024, China;
2. Key Laboratory of Space Active Opto-Electronics Technology, Shanghai Institute of Technical Physics, Chinese Academy of Sciences, Shanghai 200083, China;
3. University of Chinese Academy of Sciences, Beijing 100049, China)

Abstract: Video spectral imaging technology is an important direction in the development of remote sensing detection. It can achieve 4-dimensional information acquisition (two-dimensional space + spectrum + time), which is of great significance for application such as dynamic target detection. The current technical means are mainly based on the filter method, and do not have the high-resolution advantage of grating. Uncoupled Slit Array Scan Hyperspectral imager (uSASHI) and Coded Slit Array Scan Hyperspectral imager (cSASHI) are proposed in this paper, both use multiple slits to achieve simultaneous acquisition of multiple fields of view information to improve the information acquisition rate, and enables video-level spectral imaging. The information obtained by each slit of uSASHI will not be coupled, and *n* slits can achieve *n* times the improvement of information acquisition efficiency. The slits of cSASHI are arranged according to the compressed sensing theory, which can achieve under-sampling conditions (sampling rate $\alpha \leqslant 1$) video spectral imaging, the information acquisition efficiency can be improved by n/α times. The system designed in this paper finally realizes the 1024*490*30 spectral data cube 10 Hz video spectral imaging method, and cSASHI achieves a higher frame rate. The proposed system provides a new direction for the video spectral imaging technology and lays a better foundation for future applications.

Key words: video spectral imaging, computational imaging, compressed sensing, remote sensing

基于多视场狭缝的高效信息获取光谱成像系统

刘世界[1,2], 张星宇[1], 周 浩[1], 李春来[1,2], 李东景[1], 亓洪兴[1,2*], 王建宇[1,2,3*]

(1. 国科大杭州高等研究院,浙江 杭州,310024;
2. 中国科学院上海技术物理研究所 空间主动光电技术重点实验室,上海 200083;
3. 中国科学院大学,北京 100049)

摘要:视频光谱成像技术是目前遥感探测发展的一个重要方向,可以实现4维信息获取(两维空间+光谱+时间),对于动态目标探测等应用场景有十分重要的意义。目前的技术手段是以滤光片方式为主,不具备光栅作为分光元件时的高光谱分辨率优势。基于此,提出了非耦合狭缝阵列扫描光谱成像(uSASHI)和编码狭缝阵列扫描光谱成像(cSASHI)系统,通过增加狭缝数目的方式,实现同一时刻多个视场信息的获取,极大地提升信息获取效率。uSASHI的每个狭缝获取信息之间不会耦合,n条狭缝可以实现n倍的信息获取效率的提升,cSASHI的狭缝按照压缩感知理论排列,可以实现欠采样条件下(采样率$\alpha \leqslant 1$)视频光谱成像,信息获取效率可以提升n/α倍。本文设计的系统最终实现了1024*496*30的光谱数据立方体10 Hz视频光谱成像方式,cSASH实现了更高帧频。所提系统为视频光谱成像技术提供了新的方向,为未来动态目标探测等应用打下了基础。

Received date: 2022-06-21, **revised date**: 2022-11-07 **收稿日期**:2022-06-21,**修回日期**:2022-11-07

Biography: LIU Shi-Jie(1989—), male, Shangqiu, Henan Province, Postdoctoral fellow, research fields include compressed sensing, spectral imaging and computational imaging. E-mail: liushijie@ucas.ac.cn

* **Corresponding authors**: E-mail: qihongxing@ucas.ac.cn; jywang@mail.sitp.ac.cn

关　键　词: 视频光谱成像; 计算成像; 压缩感知; 遥感
中图分类号: TP751　　**文献标识码**: A

Introduction

The satellite-based hyperspectral imaging technology was one of the important optical remote sensing methods for Earth observation, and it is increasingly recognized by the remote sensing community because of its ability to acquire spectral and image information in three dimensions simultaneously. Hyperspectral imaging systems in traditional remote sensing can be roughly divided into two categories: the push-broom scanning hyperspectral imaging (PSHI) system and the staring hyperspectral imaging (SHI) system. The PSHI system used gratings or prisms, while the SHI system used a tunable optical filter as a splitting device. The latest representative PSHI systems are OSIRIS-REx Visible and Infrared Spectrometer (OVIRS)[1], Advanced Hyperspectral Imager (AHSI)[2]. In addition, there are Environmental Mapping and Analysis Program (EnMAP) hyperspectral imager, NASA Hyperspectral InfraRed Imager (HyspIRI). In the field of deep space exploration, there are also some typical hyperspectral imagers, such as Compact reconnaissance Imaging Spectrometer for Mars (CRISM) on Mars Reconnaissance Orbiter (MRO) and the OSIRIS-REx Visible and InfraRed Spectrometer (OVIRS). MicrOmega[3], Visible & Near Infrared Spectrometer (VNIS) onboard Yutu-2[4] are SHI systems. PSHI can achieve high spectral resolution, because of the use of gratings or prisms, but it is push-based form of platform or scanning mirror makes it only suitable for applications that are carried on mobile platforms, such as airborne and space-borne applications. The StHI system is suited to the detection in-situ, but it has failed to achieve high spectral resolution. It is because those tunable filter devices (e. g. , Acousto-optical tunable filter) are not equipped with excellent dispersion capabilities.

As the performance requirements of hyperspectral technology gradually increase, it is desired to simultaneously combine high detection sensitivity, high spatial resolution, high spectral resolution, and high temporal resolution. And the above two ways were obviously difficult to achieve. The development of snapshot hyperspectral technology with face-field imaging capability is increasingly focused on, and various new spectroscopic techniques have emerged. It can acquire spatial information and spectral information simultaneously in one sampling period directly or through recovery algorithms. Bowen's integrated field spectral (IFS) imaging technique, based on polygon mirror integration, was the first proposed snapshot spectral imaging concept[5]. This was followed by computed tomography spectroscopy (CTIS)[6-7], Fourier-based hyperspectral imager (FHI), based on the Michelson interferometer[8], the multispectral Sagnac interferometer (MSI)[9], image mapping spectrometer (IMS)[10], and image-replicating imaging spectrometer (IRIS)[11]. In addition, there are spectral imaging systems based on filter arrays and continuous tunable filters (CVF). One example is the optically replicating and remapping imaging spectrometer (ORRIS)[12]. With the proposal of computational information processing theory, such as compressed sensing[13-14], snapshot imaging spectrometers based on coded aperture have emerged. They include coded aperture snapshot spectral imagers (CASSI)[15-17], compressive sensing hyper-spectral imagers (CHSI)[18], compressive hyper-spectral imaging by random separable projections in both the spatial and the spectral domains (CHSISS)[19], and systems that have evolved on this basis. These systems use a two-dimensional random coding board to modulate the target information to achieve "compressed sensing," and use the reconstruction algorithm to recover all spectral and spatial information.

This paper firstly intends to propose a slit-scanning hyperspectral imaging (SSHI) system. Instead of being driven by the movement of the platform or scanning mirror, the slit is moved and the one-dimensional spatial information perpendicular to the slit is scanned. This allows the apparatus to detect the in-situ scene while keeping the instrument stationary. On the other hand, the SSHI system has the same components as the PSHI system except for the addition of a moving slit, which maintains the advantage of using a grating, prism, or the like, that is, high spectral resolution can be guaranteed. On this basis, Uncoupled Slit Array Scan Hyperspectral imager(uSASHI)is proposed whose time-resolution is improved. Go a step further, Coded Slit Array Scan Hyperspectral imager(cSASHI)is proposed. Its multiple slits are combined into a coding array, and the system obtains the encoded information of the detection target. Coding is transformed by moving the micro-displacement platform to improve the sampling rate. cSASHI has a similar acquisition and recovery process as the CASSI system. The difference is that we have changed the two-dimensional random coding into the slit's combination coding, so that the coding board only needs one-dimensional movement. This makes the mathematical model easier to establish as coding complexity becomes lower, and engineering is easier to implement.

1　Multi-field-of-view slit spectral imaging model

The SSHI system is proposed here first. Hyperspectral imaging technology ultimately must acquire two-dimensional spatial information and one-dimensional spectral information. Since existing devices only have two-dimensional detection capability, three-dimensional information acquisition needs to be completed by spatial scanning or temporal scanning. The essence of spatial scanning is the completion of the inter-movement of the target 2D spatial information with the imaging detector. As mentioned above, hyperspectral imagers based on push-

broom imaging type are currently the mainstream solution in aerospace. And what they accomplish is the relative motion of the entire imaging system to the target. In fact, in addition to scanning with the help of platform motion or scanning mirror, 3D data cube acquisition can also be achieved by using slit movement scanning. As shown in Fig. 1, the system is distinguished from the conventional PHI system. It is referred to here as a single slit scan imaging spectrometer system (SSHI. Slit Scan Hyperspectral imager). Unlike PHI, where the whole system moves relative to the target in a different way, SSHI accomplishes the relative motion of the slit to the detector. This is the essential difference between the two approaches.

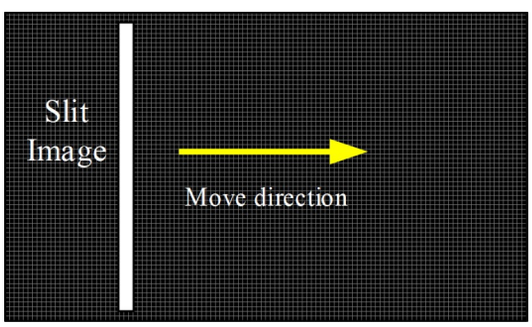

Fig. 1 The schematic diagram of the detector display under the slit scanning mode of the SSHI system
图1 SSHI系统狭缝扫描模式下的探测器示意图

SSHI achieves spatial self-scanning, which can eliminate the need for platform pushing and scanning or scanning mirror scanning, and the entire spectral imaging instrument can remain stationary for system detection. The SSHI and PHI can use the same optical components except for the addition of a control module for continuous conversion slit control, i. e. , the high-resolution characteristics of the grating and prism can be maintained. In SSHI, it has step or continuous scanning. For each unit distance the system moves, the two-dimensional information received by the detector (one-dimensional space and one-dimensional spectrum) will move one image element in the corresponding direction, i. e. , the different field-of-view positions of the detection target correspond to different positions in the detector dispersion direction. Ultimately, it is necessary to obtain a data cube by determining the spatial location and spectral position of the spectral data, and then stitching them together.

In the SSHI system, the speed of the slit shift scan is determined by the detector frame frequency and pixel size. If the slit moving speed is v, the detector frame frequency is f, and the pixel size is d, then $v = d \times f$. This has the same computational relationship as the speed of the platform in PHI.

For a data cube of $M \times N \times L$ (horizontal × vertical × spectral), the slit must be moved N times in the dispersion direction to complete the acquisition of all information. The effective detection area of the detector, i. e. , the specification should be at least $M \times (N + L - 1)$. The acquisition time of the whole data cube is N/f for a detector with a frame frequency of f. In other words, SSHI can be considered as a video hyperspectral imager with f/N frame frequency detection, which is sufficient for some scenarios.

The SSHI system achieves the acquisition of spectral information at different line-of-view positions by a single slit scan, and one detection time unit corresponds to one line-column field of view. In fact, without changing the optical system and detector system, the scanning efficiency can be greatly improved by changing a single slit into multiple slits and achieving simultaneous scanning of multiple slits to obtain spectral information. The arrangement of the slits ensures that the dispersions corresponding to adjacent slits do not overlap. That is, the interval between the two slits is at least L image elements in size under the condition that the slit-to-detector optical imaging ratio is 1:1, while not considering different dispersions corresponding to different fields of view. Usually, due to reasons such as non-ideal factors of optical components, such as the cut-off wavelength position of the cut-off filter still exists part of the energy. It is necessary to set the adjacent slit interval appropriately larger than L to avoid the occurrence of spectral mixing of different fields of view. The system is called the uncoupled Slit Array Scanning Spectral Imaging System (uSASHI, Uncoupled Slit Array Scan Hyperspectral imager). The distance between two adjacent slits is D image elements, and there are P slits in the slit array, and there exists the relationship: $N \approx PD$. The whole slit array only needs to move D image elements to achieve the acquisition of information corresponding to the whole field of view. The scanning efficiency can be improved $N/D(\approx P)$ times compared to SSHI. Apparently, SASHI is a video hyperspectral imaging system with a frame rate of f/D, which is about P times the frame rate of SSHI. Obviously, this is a major enhancement and greatly expands the usefulness of the system.

The SSHI and uSASHI systems have a one-to-one correspondence between the detector image element reception information and the target information, and the information is processed under the Nyquist sampling theorem. In fact, compressive sensing as a novel information processing theory can inspire us to explore new imaging systems. The slit arrays are arranged via a certain coded form rather than at equal intervals, the detector's single acquisition is a superposition of spectral imaging information from multiple slits at different locations. The system maps the 3D data cube onto the 2D detector surface array, forming a mixed stack of encoded information and realizing data dimensionality reduction. The set encoding form corresponds to the detection matrix to be created. The established detection matrix should satisfy the Restricted Isometry property (RIP), which is necessary to obtain the full information, if it corresponds to the appropriate vectorized detection data. The acquisition of the full spatial spectral image can be achieved by a suitable reconstruction algorithm. The system is called the coded slit array scanning spectral imaging system

(cSASHI, Coded Slit Array Scan Hyperspectral imager).

Since the dispersion only occurs in the horizontal direction, and the vertical direction does not participate in encoding, only one line of data is analyzed for the sake of simplicity[22]. Fig. 2 shows the process of constructing a solution model for a cube of 1×4×3. c_{ijl} stands for the i_{th} row, j_{th} column, and the l_{th} spectral band of data cube $\boldsymbol{C}$. m_{ik} stands for the i_{th} slit position data (0 or 1) in code mask $\boldsymbol{M}$ of the k_{th} sample, and the detector $\boldsymbol{D}$ receives data as d_{ijk} which is the data of the i_{th} row and the j_{th} column on the detector of the k_{th} measurement.

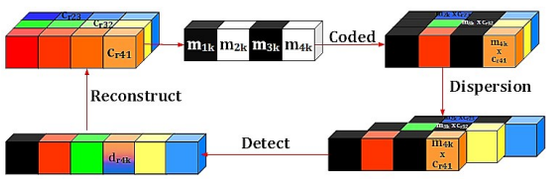

Fig. 2　The process of constructing a solution model
图2　构建方法模型的过程

As shown in Fig. 3:

$$\boldsymbol{m}_k = \left[m_{4k}, m_{3k}, m_{2k}\right], \boldsymbol{c}_1 = \left[c_{r41}, c_{r32}, c_{r23}\right]^T$$

Then:

$$d_{r4k} = \boldsymbol{m}_k \boldsymbol{c}_1$$

Written as:

$$\boldsymbol{d}_{r4} = \left[d_{r41} \ldots d_{r4k} \ldots d_{r4p}\right]^T, \boldsymbol{m} = \left[\boldsymbol{m}_1 \ldots \boldsymbol{m}_k \ldots \boldsymbol{m}_p\right]^T$$

Then:

$$\boldsymbol{d}_{r4} = \boldsymbol{m}\boldsymbol{c}_1 \quad . \quad (1)$$

Equation (1) shows the computing relationship between sample $\boldsymbol{d}_{r4}$ and target information $\boldsymbol{c}_1$. The other corresponding vectors have the same construction process. In the case of under-sampling, $\boldsymbol{m}$ is a "fat matrix", which has a few rows smaller than the number of columns. When $\boldsymbol{m}$ satisfies the RIP, the above matrix becomes a compressed sensing measurement model, and $\boldsymbol{c}_1$ can be reconstructed by a refinement algorithm such as sparse optimization[17-18]:

$$\hat{\boldsymbol{c}}_1 = \arg\min_{\boldsymbol{c}_1} \left(\left\| \boldsymbol{d}_{r4} - \boldsymbol{m}\boldsymbol{c}_1 \right\|_2^2 + \tau \left\| \boldsymbol{c}_1 \right\|_l \right) \quad . \quad (2)$$

When $\boldsymbol{m}$ is full rank, it corresponds to a full sampling situation:

$$\hat{\boldsymbol{c}}_1 = \boldsymbol{m}^{-1}\boldsymbol{d}_{r4} \quad . \quad (3)$$

Which is equivalent to:

$$\hat{\boldsymbol{c}}_1 = \arg\min_{\boldsymbol{c}_1} \left(\left\| \boldsymbol{d}_{r4} - \boldsymbol{m}\boldsymbol{c}_1 \right\|_2^2 \right) \quad . \quad (4)$$

Under one exposure, cSASHI has the same effective detection area as the SSHI detector. When n coding measurements are performed, the corresponding sample data amount is $n \times M \times (N + L - 1)$. The sampling rate is $(n \times (N + L - 1))/(N \times L)$, and the duration of an entire data cube is n/f. So, cSASHI system can be seen as a hyperspectral video imager with a frame rate detection capability of f/n. As $n \leqslant N$, cSASHI usually has a higher detection frequency than SSHI. It can be seen from the mathematical model that the information obtained by one exposure of the cSASHI system is the linear sum of several single sampling results in SSHI. This guarantees the feasibility of the mathematical model.

It should be noted that the imaging field of view in an optical imaging system is limited, and the design also tends to preserve a better portion of the image quality by limiting the field of view. Therefore, in the encoding system, it is sufficient to ensure that the information in the field of view is encoded. An appropriately sized encoding mask can be set up to match the field-of-view diaphragm so that the encoding sub-region strictly matches the position of the imaging field-of-view region. This subregion is obviously smaller than the area of the mask plate. By moving the mask while the diaphragm, which is used to limit the field of view, remains unchanged, the "code" for the location of the imaging area will change, thus achieving multiple exposures with different codes. Fig. 3 shows the schematic diagram of the three spectral imaging methods.

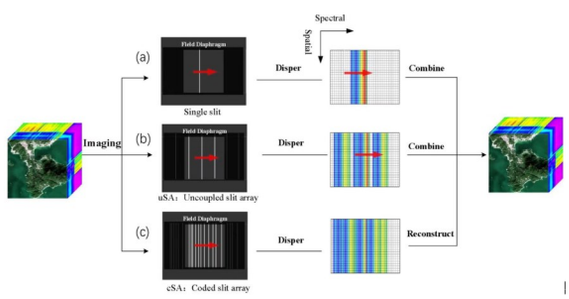

Fig. 3　Comparison of three spectral imaging methods, (a) the slit scanning mode of the SSHI system, (b) the uncoupled slit array scanning of uSASHI, (c) the coded slit array scanning of cSASHI
图3　三种光谱成像方式比较, (a) SSHI, (b) uSASHI, (c) cSASHI

2　Imaging experiment system

2.1　Overview

The schematic diagram and mechanical structure design diagram of the 2-imaging experiment system are shown in Fig. 4 and Fig. 5, respectively. The system is divided into a panchromatic imaging channel (with high spatial resolution) and a spectral imaging channel through the dichroic sheet. The two can form a good complement of information and are both good data sources for applications such as imaging and detection. As mentioned above, the image modulator is located at the primary image plane of the imaging system, and can have different forms to achieve different information acquisition methods.

The design parameters of this system are shown in the following table.

The core of the system is the spectral imaging channel, which mainly consists of the spectrometer assembly and the front optical path combined by the telescope and the relay mirror set. In order to meet the specificity of the computational optics, it is necessary to expand the traditional push-scan type line-field spectrometer into a snap-

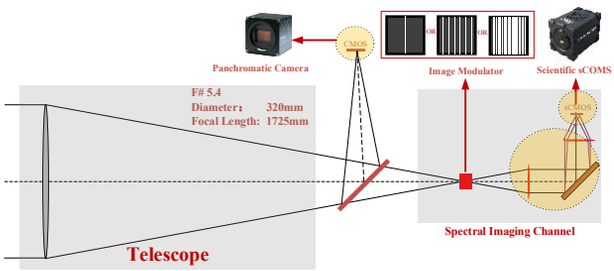

Fig. 4 The schematic diagram
图4 系统原理图

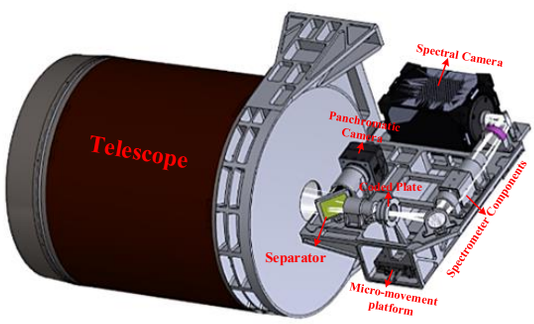

Fig. 5 Mechanical design
图5 机械结构设计

Table 1 Specifications of the system
表1 系统参数

Parameters	Panchromatic imaging channel	Spectral imaging channel
Wavelength	0. 45~0. 85 μm	0. 45 ~ 0. 9 μm
Focal length	1 725 mm	1 725 mm
Working F number	5. 5	5. 5
Spectral sampling	—	15 nm
Field of view	±0. 370°×±0. 278°	±0. 221°×±0. 111°
Spatial resolution	0. 002 mrad (1 m@500 km)	0. 007 6 mrad (3. 8 m@500 km)
Spectral resolution	—	18 nm
Spectrometer magnification	—	1×
Detector array size	6 464×4 852	1 024×512
Detector pixel size	3. 45 μm	13 μm

shot type face-field spectrometer. At this time, the object surface of the spectrometer is extended in the spectral direction and is rectangular. It also changes from a single slit to a movable array of coded slits, requiring a larger field of view along the track compared to ordinary imaging spectrometers. The parameters of the designed spectrometer components are shown in Table 2, and the specific components are shown in Fig. 6, which mainly consist of a collimating mirror set, a focusing mirror set, and a prism pair used as a beam splitting element. The use of prisms as beam splitting elements can effectively avoid the overlap between the advanced sub spectrum of the grating and the signal light of the same wavelength in different along-track fields of view. Although its spectral dispersion has a certain nonlinearity, the signal energy is strong, while prism pairs of different material combinations can be used to reduce the smile and keystone of the spectrometer. The system is designed to use N-BAF3 as well as N-BASF64 in Schott glass for matching, as shown in Fig. 8, to obtain a better spectral effect. The collimator and focus mirror use a spherical lens set to meet the needs of a larger field of view. The converging light at the primary focal plane of the front optical path of the telescope is changed to parallel light by the collimator set to ensure the consistency of the prism pair splitting. After using prism spectroscopy, secondary imaging and aberration compensation are performed by the focusing mirror set to obtain better multispectral blended images for subsequent data processing.

Table 2 Specifications of the spectrometer components
表2 光谱仪器件参数

Parameters	Spectrometer components
Spectral range	0. 45 ~ 0. 9 μm
Spectrometer magnification	1×
Object size	±6. 656 mm×±3. 328 mm
Spectroscopic element	Prism pairs
Spectral sampling	15 nm
RMS radius of spot	≤4. 5 μm
Smile	<3. 1 μm
Keystone	<4. 2 μm
MTF(@38. 46 lp/mm)	>0. 73@0. 45 μm; >0. 73@0. 65 μm; >0. 69@0. 9 μm

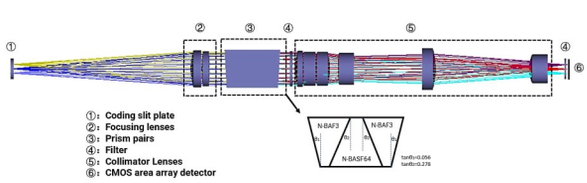

Fig. 6 The optical layout of the spectrometer components
图6 光谱仪光学结构

The image modulation components are realized by laser etching on the chrome-plated quartz substrate, and the etching accuracy can reach 0. 1-micron level, which can well meet the system accuracy requirements. At the same time, the quartz substrate has a good optical utilization rate in the visible band, and the chromium layer has a good light blocking effect, so the component has a good contrast performance.

3 Experiments and results

3. 1 Calibration

The system still uses the traditional monochromatic parallel light calibration method for spectral calibration. The difference is that this system is a multi-field spectral

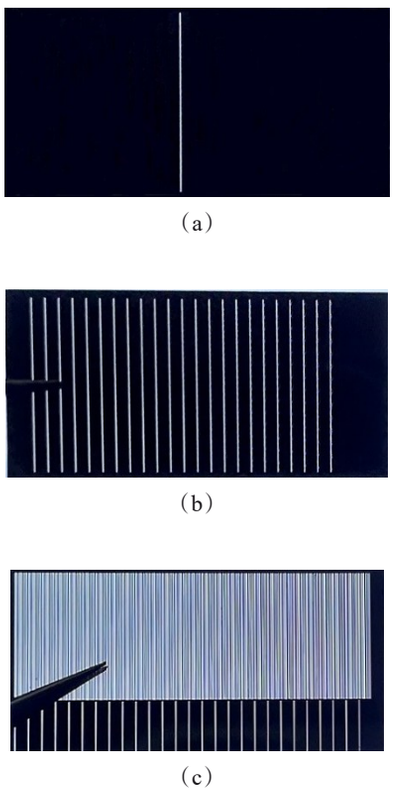

Fig. 7　Physical view of different types of slits (a) single slit, (b) uniform array slit, (c) coded array slit
图 7　不同类型狭缝实物图(a)单狭缝,(b)均匀阵列狭缝,(c)编码阵列狭缝

imaging system in the spectral dimension. The imaging quality and spectral performance of different fields of view are different, and even have great differences, such as the most peripheral field of view and the center field of view. The calibration for each field of view can obtain very accurate calibration data. However, due to the large number of fields of view and the small single-color step size required for calibration, a lot of calibration data will be generated and need post-processing. The central wavelength or bandwidth corresponding to the field of view at different positions in the spectral dimension direction has a certain relationship. This relationship can be easily obtained by linear or nonlinear fitting. Therefore, it is often necessary to select several representative fields of view positions for spectral calibration. The central wavelength or bandwidth of other positions can be linearly interpolated.

The standard monochromator is HORIBA′s iHR320 when calibrating, using halogen tungsten lamp as light source, and with parallel light path, the monochromator′s light output slit width is 0. 1 mm, the scanning step is 0. 5 nm, and the wavelength scanning range is 450~900 nm. After calibration, the spectral resolution calibration, and fitting results at the center of the field of view are shown in the figure below.

The system uses multiple slits for surface target imaging. Different positions of the surface target will enter the optical system with different angles of incidence. In order to reduce the influence of dispersion inconsistency, the prism is installed in the optical system at the minimum deflection angle. Position, which is often a way to reduce sensitivity to non-parallelism of incident light rays. The spectral calibration of 5 different fields of view was carried out respectively. From the data fitting effect of center wavelength and spectral resolution, the spectral dispersion characteristics of different fields of view are almost the same.

In fact, even with large inconsistencies across different fields of view, spectral position and resolution can be quantified simply by calibration. Another aspect is the quantification and calibration of smile quantification. As shown in the table, the spectral curvature data of the three fields of view are given, and the smile of the system is not very large.

As for the radiation calibration: It can be seen from the above system model that the corresponding relationship between the received data of the uSASHI detector and the target radiation is clear, just like PHI. The data received by the detector in the cSASHI system is the linear superposition of the corresponding single information elements, so the radiation calibration of the system proposed in this paper has no special requirements with the traditional method.

3. 2　Imaging results

3. 2. 1　Indoor imaging

Small telescopes are used (F#1, f: 18 mm) in indoor experiments, to solve and verify problems that may arise in engineering practice.

Synchronized exposure settings for mechanical mod-

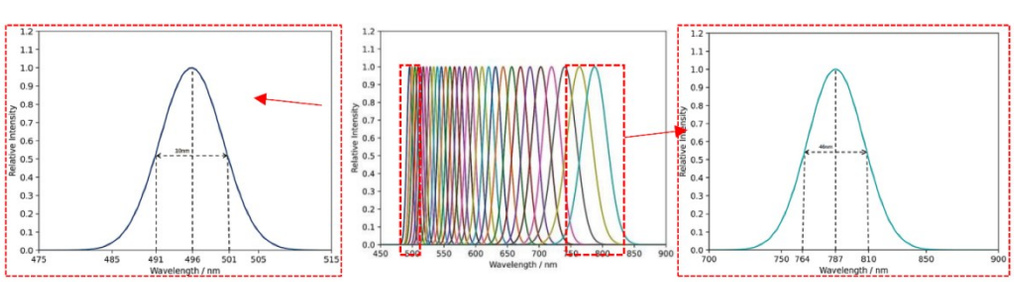

Fig. 8　Center field spectral calibration results
图 8　中心视场光谱定标结果

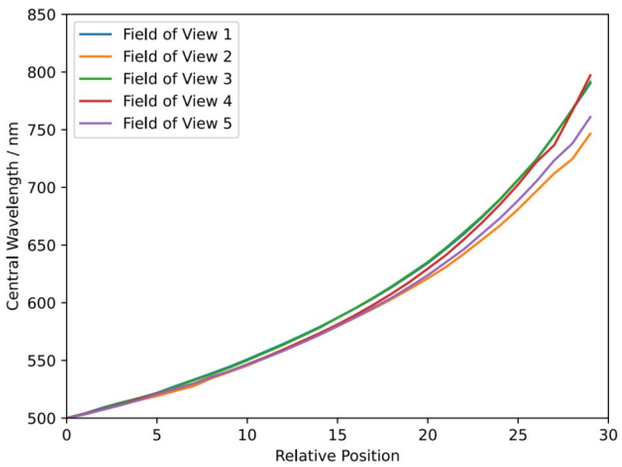

(a)

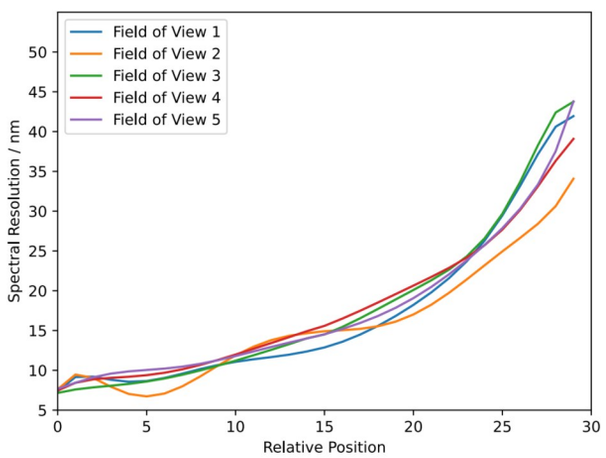

(b)

Fig. 9 Spectral calibration results for 5 typical fields of view (a) center wavelength, (b) spectral resolution
图9 五个视场光谱定标结果 (a)中心波长,(b)光谱分辨率

Table 4 Smile of the system
表4 系统smile光谱畸变

Slit position	Wavelength	Smile/mm
Top edge	450 nm	0. 003 56
	650 nm	0. 002 84
	850 nm	0. 002 67
Centre	450 nm	0. 002 95
	650 nm	0. 004 44
	850 nm	0. 004 86
Bottom edge	450 nm	0. 002 95
	650 nm	0. 004 44
	850 nm	0. 004 86

ulator and detector information acquisition in the proposed system are critical for imaging. The micro motor can have two modes: continuous movement and step movement. In the continuous system mode, the slit continuously scans the image surface of the target, which is like the information acquisition method of traditional PHI. The only difference is that PHI scans the object surface, which does not affect the essential correspondence of information acquisition. In the step movement mode, a detector unit and the ground imaging unit have a clearer one-to-one correspondence, so the system adopts the latter method, and the micro-motor moves one pixel and sends a pulse signal, trigger the detector exposure.

On the other hand, during the imaging process, the movement of the micromotor has non-uniformity, which will lead to non-uniform response of the detector to receive information. The Fig. 10(c) shows the imaging results caused by this reason, while Fig. 10(a) is the imaging target, and Fig. 10(b) is the sampling data of a certain frame on the detector. Fortunately, we can obtain the precise movement curve of the displacement motor, and fully adjust the exposure difference caused by the difference between the actual moving position curve and the ideal curve, which can achieve very good image correction, this step is called synchronization correction.

(a)

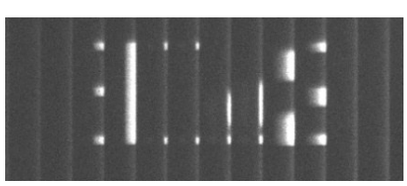

(b)

(c)

Fig. 10 Imaging objectives and preliminary imaging results (a) RGB Image, (b) sampling images, (c) imaging without synchronization correction
图10 成像目标和初步成像结果 (a)彩色图像,(b)采样图像,(c)未经过同步校正的成像结果

An integrating sphere that can be traced to a standard source is used as the illumination source. When the micromotor moves 13 μm, a pulse signal is sent, which is the exposure trigger signal of the detector. The exposure of the detector is completed, and the next unit information acquisition cycle is started. That is, the sampling

frame rate *Fr* of the system depends on the motion period T of the micro-motor and the exposure time τ of the detector: $Fr=1/(T+\tau)$. In the experiment, the V-408 high-precision motor of PI company is used as the moving part, the maximum moving speed can reach 1. 1m/s, and the displacement accuracy can reach 1 μm. By setting the speed, T=1ms is achieved, and τ=9 ms is set according to the brightness of the scene, that is, the system achieves a sampling frame rate of 10 Hz, which is the imaging frame rate of cSASHI, and the imaging frame rate of uSASHI can be higher, as mentioned above.

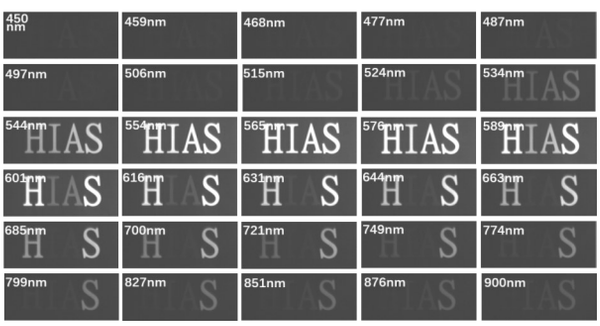

Fig. 11　Different wavelength images
图 11　不同波长图像

The reflectivity profiles in different wavelengths are important features for detecting targets. Because the light source is traceable, the reflectivity of the target can be well inverted. As shown in Fig. 11. Their peak wavelengths are 600 nm and 580 nm, respectively. This is in accordance with the actual.

3. 2. 2　Outdoor imaging

The system is designed for remote sensing applications, and large telescopes are used for long-range imaging, with test targets approximately 500 m away. The panchromatic and spectral channels of the system are simultaneously imaged, and after a simple atmospheric correction, as shown in the figure, the structure of the panchromatic imaging and the imaging results of the 30 spectral channels of uSASHI are given.

The spatial resolution of the spectral imaging channel is about 4 times that of the panchromatic channel, and the two channels can realize the complementation of spatial information and spectral information. The spatial resolution of spectral imaging in this experiment is 512×245, and the panchromatic channel achieves 2560×2450 information acquisition. Part of the imaging results are shown in Fig. 14. The panchromatic channel obtains high spatial resolution data. According to the design, the field of view is about 5×5 times that of the single imaging of the spectral imaging channel. The data obtained by the latter is the "sub-field of view" spectral data of the former. "Scanning" can obtain more dimensional information of the corresponding target in a targeted manner, that is to say, the panchromatic channel can realize an overview, and the spectral channel can realize further fine detection based on this, which can play a crucial role in many application scenarios. As mentioned above,

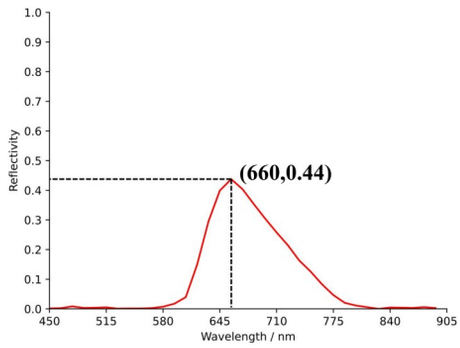

（a）　Position 1

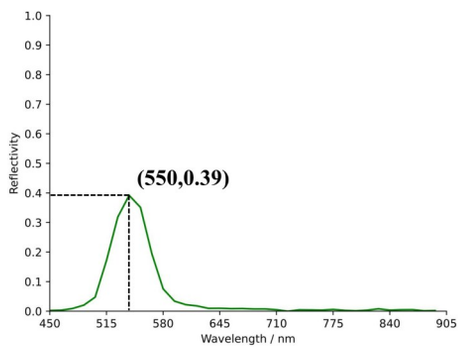

（b）　Position 2

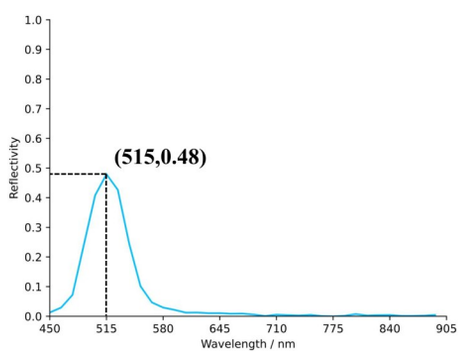

（c）　Position 3

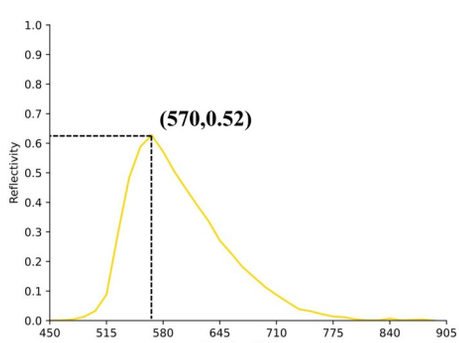

（d）　Position 4

Fig. 12　Reflectance curves (a)~(d): reflectance curves corresponding to positions 1~4 respectively
图 12　反射率曲线(a)~ (d):分别对应位置 1~4 的反射率曲线

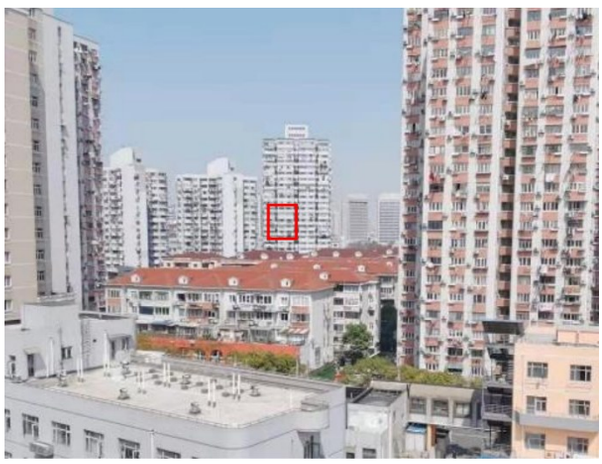

(a)

(b)

Fig. 13 Outdoor imaging physical picture (a) target in the red box, (b) system physical
图13 室外成像实物图 (a)红框内为目标,(b)系统实物

(a)

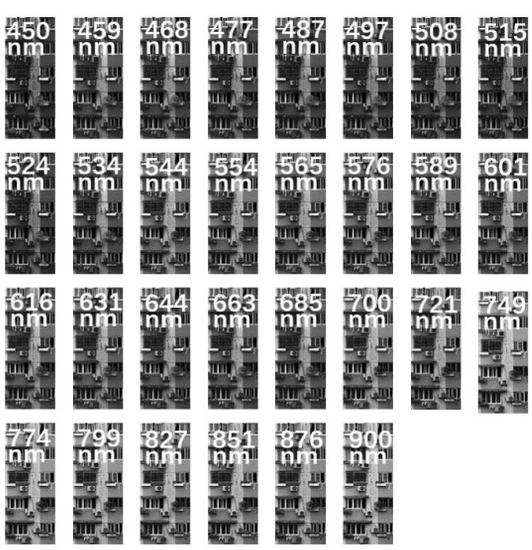

(b)

Fig. 14 Outdoor panchromatic channel imaging and spectral imaging results (a) panchromatic channel imaging, (b) single-band image of 30 channels
图14 室外全色通道成像和光谱成像结果 (a)全色通道成像,(b) 30个通道的单波段图

uSASHI and cSASHI are two high-efficiency information acquisition systems, which have video characteristics. With the same settings, the system can achieve 10 Hz video spectral imaging. As shown in Fig. 15 and Fig. 16 (b), dynamic target in the imaging scene (wind-swept tree) is selected . The results of partial video spectral imaging in one second are given. The figure shows the spectral imaging results of a certain frame of cSASHI under the conditions of 60%, 70%, 80%, 90%, and 100% sampling rates, respectively. The corresponding imaging frame frequencies are 16.6 Hz, 14.3 Hz, 12.5 Hz, 11 Hz, 10 Hz.

4 Conclusions

In summary, we investigated the imaging methods via comparative study of single slit, uncoupled slit arrays, and coded slit arrays. We achieved frame rate 10 Hz for uncoupled slit array spectral imaging and up to 16.6 Hz frame rate transmission characteristics for coded slit array spectral imaging at five sampling rates. The slit array coding is used to replace the line field of view with a surface field of view and to increase the sampling efficiency, ultimately increasing the speed of spectral imaging of external dynamic targets, A new type of spectral imaging system was then realized. The system proposed in this paper uses a prism as the spectroscopic device, which can be replaced by a grating or a combination of the two in future research, retaining the advantages of high spectral resolution of the spectroscopic device to accommodate more applications. The essence of uSASHI is to collect and process information under the traditional information processing framework. It can realize flexible

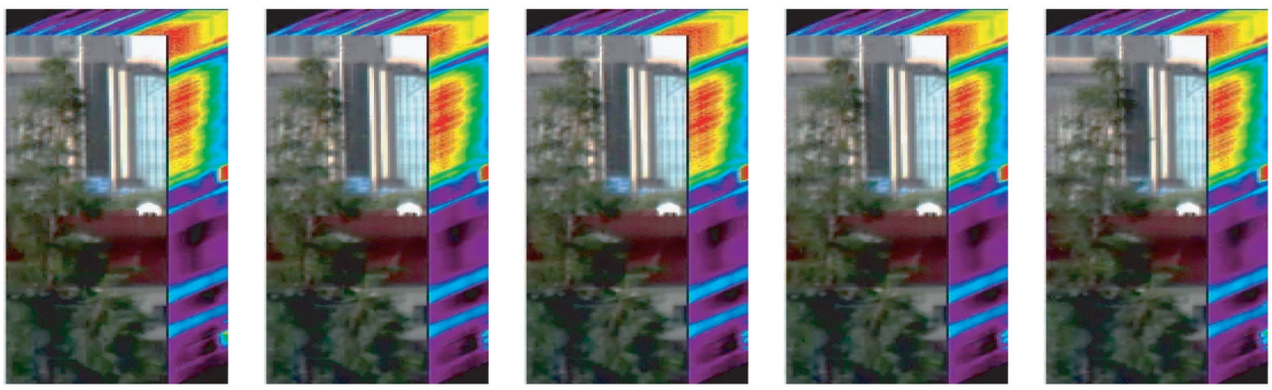

(a)2 frame　(b)4 frame　(c)6 frame　(d)8 frame　(e)10 frame

Fig. 15　Results of 10 Hz video spectral imaging implemented by uSASHI (a)-(e) are the results of continuous 1s spectral imaging(half of them)

图 15　uSASHI实现的 10 Hz视频光谱成像结果(a)-(e)为连续 1s中的光谱成像结果(其中一半)

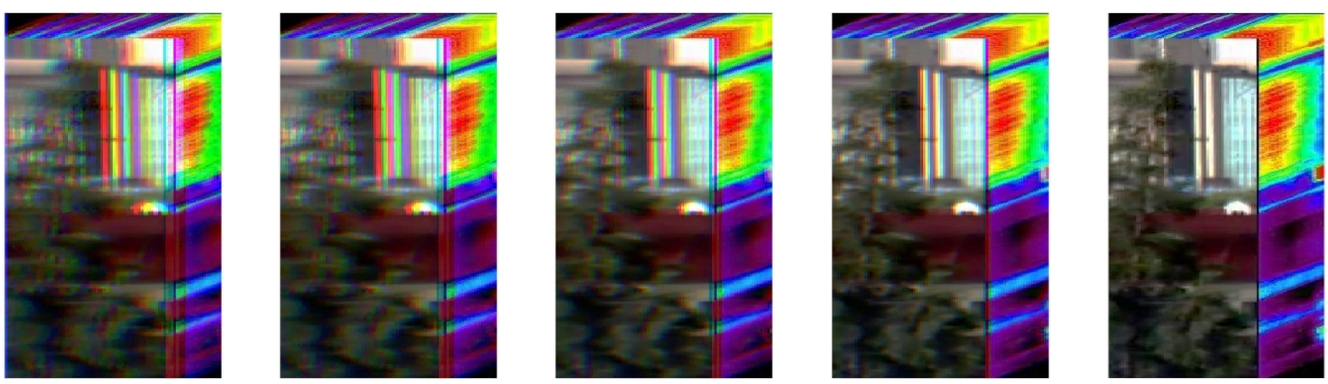

(a)　(b)　(c)　(d)　(e)

Fig. 16　Spectral imaging results of cSASHI at different sampling rates (a)-(e) Spectral imaging results at 16.6 Hz for 60% sampling rate, 14.3 Hz for 70% sampling rate, 12.5 Hz for 80% sampling rate, 11 Hz for 90% sampling rate, and 10 Hz for 100% sampling rate, respectively

图 16　cSASHI不同采样率条件下的光谱成像结果(a)-(e)分别为 60% 采样率的 16.6 Hz, 70% 采样率的 14.3 Hz, 80% 采样率的 12.5 Hz, 90% 采样率的 11 Hz, 100% 采样率的 10 Hz的光谱成像结果

conversion of spatial, spectral and temporal resolutions by adjusting system parameter settings. It is suitable for application scenarios that require high reliability of remote sensing data. cSASHI is based on the sparsity of imaging data, information acquisition under the framework of compressed sensing, an emerging information theory, can achieve higher data acquisition efficiency than uSASHI, and will lose some detailed information, but can retain the principal component information of the target, which is suitable for dynamic targets, scenarios such as tracking and recognition, which do not require complete information. In addition, the modulation component of the system acquires information by scanning, which can achieve good information acquisition for static targets, but it is unavoidable that there will be problems caused by the difference in scanning time for dynamic target scenes. The adjustment of the synchronization method of detector acquisition and modulator can improve this problem and is also one of the future research directions.

References

[1] Reuter D C, Simon A A, Hair J, *et al*. The OSIRIS-REx Visible and Infrared Spectrometer (OVIRS): Spectral Maps of the Asteroid Bennu [J]. *Space Science Reviews*, 2017, **214**(54): 1-22.

[2] Liu Y. Visible-shortwave Infrared Hyperspectral Imager of GF-5 Satellite [J]. Spacecraft Recovery & Remote Sensing, 2018, **39**(03): 25-28.(刘银年. "高分五号"卫星可见短波红外高光谱相机的研制[J]. **航天返回与遥感**), 2018, **39**(03): 25-28.

[3] Bibring J P, Hamm V, Langevin Y, *et al*. The MicrOmega Investigation Onboard Hayabusa2 [J]. *Space Science Reviews*, 2017, **208**(29): 401-412.

[4] Li C, Liu D, Liu B, *et al*. Chang'E- 4 initial spectroscopic identification of lunar far-side mantle-derived materials [J]. *Nature*, 2019, **569**(7756): 378-382.

[5] Gao Z D, Gao H X, Zhu Y Y, *et al*. Review of snapshot spectral imaging technologies [J]. Optics and Precision Engineering, 2020, **28**(6):1323-1343.(高泽东, 高洪兴, 朱院院, 等. 快照式光谱成像技术综述[J]. **光学精密工程**), 2020, **28**(6):1323-1343.

[6] Okamoto T, Yamaguchi I. Simultaneous acquisition of spectral image

information [J]. *Optics Letters*, 1991, **16**(16): 1277-1279.
[7] Ford B, Descour M, Lynch R. Large-image-format computed tomography imaging spectrometer for fluorescence microscopy [J]. *Optics Express*, 2001, **9**(9): 444-453.
[8] Kudenov M W, Dereniak E L. Compact snapshot birefringent imaging Fourier transform spectrometer [J]. *Proceedings of SPIE - The International Society for Optical Engineering*, 2010, 781206.
[9] Allington-Smith J. Basic principles of integral field spectroscopy [J]. *New Astronomy Reviews*, 2006, **50**(4/5): 244-251.
[10] Bodkin A, Sheinis A, Norton A, *et al*. Snapshot hyperspectral imaging: the hyper pixel array camera [J]. *Proceedings of SPIE - The International Society for Optical Engineering*, 2009, 73340H.
[11] Wang Y, Pawlowski M E, Tkaczyk T S. High spatial sampling light-guide snapshot spectrometer [J]. *Optical Engineering*, 2017, **56**(8): 081803.
[12] Mu T, Han F, Bao D, *et al*. Compact snapshot optically replicating and remapping imaging spectrometer (ORRIS) using a focal plane continuous variable filter [J]. *Optics Letters*, 2019, **44**(5): 1281-1284.
[13] Donoho D L. Compressed sensing [J]. *IEEE Transactions on Information Theory*, 2006, **52**(4): 1289-1306.
[14] Candes E J, Romberg J, Tao T. Robust uncertainty principles: exact signal reconstruction from highly incomplete frequency information [J]. *IEEE Transactions on Information Theory*, 2006, **52**(2): 489-509.
[15] Wagadarikar A A, Bones P J, Fiddy M A, *et al*. SPIE Proceedings [SPIE Optical Engineering + Applications - San Diego, California, USA (Sunday 10 August 2008)] Image Reconstruction from Incomplete Data V - Spectral image estimation for coded aperture snapshot spectral imagers [J]. 2008, 707602.
[16] Kittle D, Choi K, Wagadarikar A, *et al*. Multiframe image estimation for coded aperture snapshot spectral imagers [J]. *Applied Optics*, 2010, **49**(36): 6824-6833.
[17] Gehm M E, John R, Brady D J, *et al*. Single-shot compressive spectral imaging with a dual-disperser architecture [J]. *Optics Express*, 2007, **15**(21): 14013-14027.
[18] Sun T, Kelly K. Compressive sensing hyperspectral imager [C]. Computational Optical Sensing and Imaging. Optical Society of America, 2009: CTuA5.
[19] August Y, Vachman C, Rivenson Y, *et al*. Compressive hyperspectral imaging by random separable projections in both the spatial and the spectral domains [J]. *Applied Optics*, 2013, **52**(10): 46-54.
[20] Liu S J, Zhang X D, Zhang Y, *et al*. Multi-frame image coded aperture snapshot spectral image technology [J]. *Journal of Infrared and Millimeter Waves*, 2017, **36**(6): 799-804.
[21] Sun J, Wang S, Dong Y. Sparse block circulant matrices for compressed sensing [J]. *Iet Communications*, 2013, **7**(13): 1412-1418.
[22] Chartrand R, Yin W. Iteratively reweighted algorithms for compressive sensing [C]. IEEE International Conference on Acoustics, Speech and Signal Processing, 2008.